

Chandra Observations of Pulsar B1509–58 and Supernova Remnant G320.4–1.2

Bryan M. Gaensler¹

*Center for Space Research, Massachusetts Institute of Technology,
Cambridge MA, USA*

Jonathan Arons, Michael J. Pivovarov

University of California, Berkeley CA, USA

Victoria M. Kaspi

McGill University, Montreal QC, Canada

Abstract.

The young and energetic pulsar B1509–58 powers a bright X-ray synchrotron nebula, embedded in the unusual supernova remnant G320.4–1.2. We present observations of this system with the *Chandra X-ray Observatory*, which show a spectacularly complicated source. The nebula is dominated by a bright collimated feature which we interpret as a relativistic jet directed along the pulsar spin axis. Several compact knots can be seen in the immediate vicinity of the pulsar. While many of these features are similar to those seen around the Crab pulsar, the nebula surrounding PSR B1509–58 shows important differences which are possibly a result of the the latter’s low nebular magnetic field and low density environment.

1. Introduction

The supernova remnant (SNR) G320.4–1.2 (MSH 15–52) has unusual radio and X-ray properties. At radio wavelengths (Figure 1), its morphology is dominated by two distinct limbs of radio emission. Superimposed on the northern limb is a bright core of emission, coincident with the H α nebula RCW 89. The distinctly non-circular appearance of this source has been attributed to expansion into an elongated cavity, a claim supported by recent HI observations of this region (Dubner et al. 2002). HI absorption towards the SNR demonstrates it to be at a distance of 5 kpc (Gaensler et al. 1999).

At X-ray energies (Figure 1), the system is dominated by a bright central point source. This corresponds to the pulsar B1509–58, which has also been detected at radio wavelengths and in γ -rays. PSR B1509–58 is one of the youngest

¹Current address: Harvard-Smithsonian Center for Astrophysics, Cambridge MA, USA

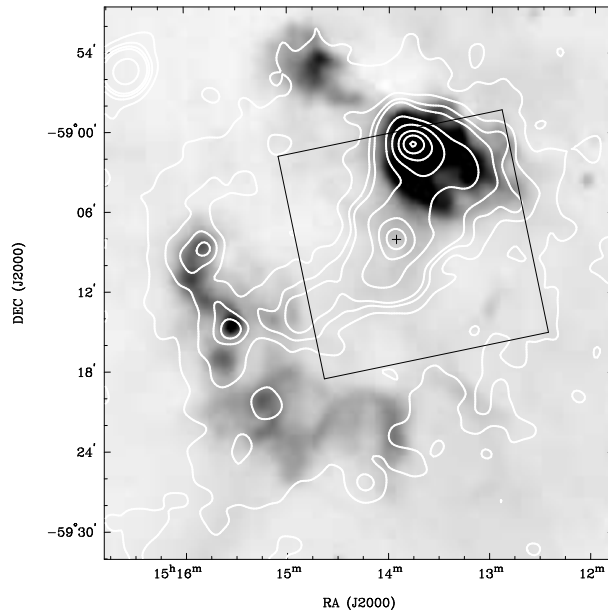


Figure 1. A radio/X-ray comparison of G320.4-1.2. The greyscale corresponds to 843-MHz MOST observations, while the white contours represent smoothed *ROSAT* PSPC data. The position of PSR B1509-58 is marked with a “+”, while the black box delineates the ACIS-I field-of-view.

and most energetic pulsars known: it has a spin-period $P = 151$ ms, a magnetic field $B = 1.5 \times 10^{13}$ G, a spin-down luminosity $\dot{E} = 1.8 \times 10^{37}$ erg s $^{-1}$ and a characteristic age $\tau = 1700$ yr. Surrounding the pulsar is an elongated non-thermal nebula, presumed to be the pulsar wind nebula (PWN) powered by the pulsar’s spin-down; no radio counterpart to this PWN has been identified. To the north of PSR B1509-58 is a source of thermal X-rays, coincident with the bright radio and optical emission from RCW 89 (Trussoni et al. 1996; Tamura et al. 1996).

Existing observations have raised a number of issues regarding this pulsar and its interaction with its environment. Firstly, the elongated morphology of the PWN suggests that its morphology is dominated by a collimated outflow directed along the pulsar spin-axis, which possibly collides with and is interacting with the RCW 89 region (Manchester & Durdin 1983; Tamura et al. 1996; Brazier & Becker 1997; Gaensler et al. 1999). Greiveldinger et al. (1995) have claimed that there is a compact disc of nebular emission immediately surrounding the pulsar, while Brazier & Becker (1997) rather propose a “cross”-shaped morphology in this region, which they interpret as an equatorial torus and polar jets, seen edge-on.

Clearly our understanding of this complicated source can benefit from observations at higher angular resolution. We have consequently carried out observations of PSR B1509-58 and its surroundings with the *Chandra X-ray Ob-*

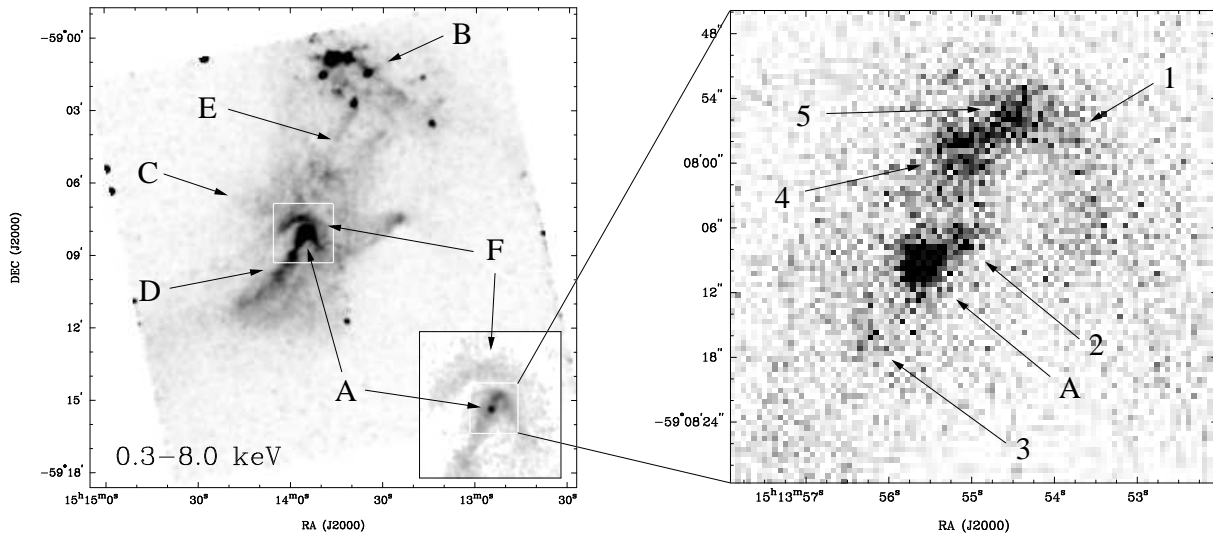


Figure 2. *Chandra* images of PSR B1509–58/ SNR G320.4–1.2 in the energy range 0.3–8.0 keV. The left-hand panel shows the entire field, exposure-corrected and convolved with a $10''$ gaussian. The white box in the main image shows the region covered by the inset at lower right. The right-hand panel shows the region immediately surrounding the pulsar. Specific features discussed in the text are indicated.

servatory. We summarize these results below; these data are discussed in more detail by Gaensler et al. (2002).

2. X-ray Observations

2.1. Imaging

PSR B1509–58 was observed with the ACIS-I detector on *Chandra* on 2000 Aug 14, with an effective exposure time of 19 ks. The resulting image is shown in the left panel of Figure 2. A number of features can be seen in this image: the pulsar itself (marked as A), a ring of X-ray clumps coincident with RCW 89 (B), a diffuse elongated PWN surrounding the pulsar (C), a “jet” feature lying along the PWN’s main axis (D), a possible counterpart to the “jet” seen as a region of *reduced* emission (E), and an arc just to the north of the pulsar which is bisected by the main nebular axis (F).

The right panel of Figure 2 shows the region immediately surrounding the pulsar at the full resolution of the data. This Figure shows an inner arc sitting inside feature F (marked as 1), and several knots close to the pulsar (2, 3, 4, 5).

2.2. Spectroscopy

We have extracted over 50 000 counts from the diffuse PWN (feature C in Figure 2); these data show no spectral features. Fitting them with a power law, we find an absorbing column $N_H = (9.5 \pm 0.3) \times 10^{21} \text{ cm}^{-2}$ and a photon index

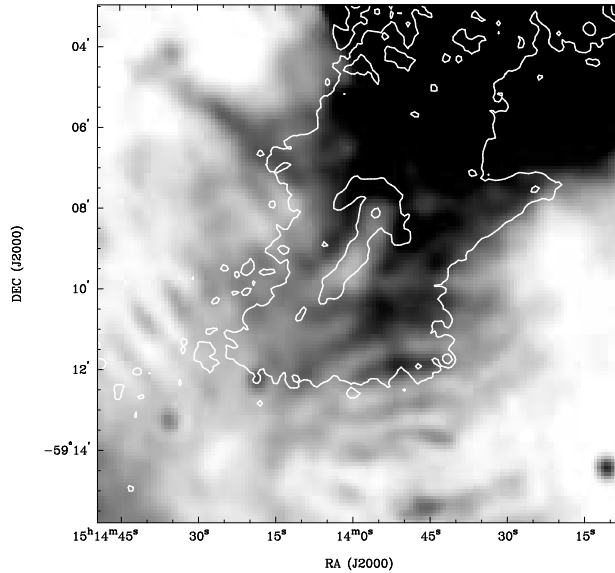


Figure 3. Radio and X-ray emission in the region surrounding PSR psr. The greyscale shows radio data from the 1.4-GHz observations of Gaensler et al. (1999), while the contours show *Chandra* data as in Figure 2, with contours at 0.5%, 2% and 30% of the peak.

$\Gamma = 2.05 \pm 0.04$, in good agreement with previous results. The brighter features superimposed on this diffuse emission all have distinctly harder spectra: the “jet” (feature D), outer arc (F) and inner arc (1) all have $\Gamma \approx 1.6 - 1.7$, while the innermost knots (2–5) all have $\Gamma \approx 1.3 - 1.6$.

The spectrum of the RCW 89 region shows several clear emission lines, confirming its interpretation as a thermal source distinct from the other components of the system (e.g. Tamura et al. 1996). Preliminary analysis of these data shows that the emission can be approximately fit by a non-equilibrium ionization model with variable abundances.

3. Discussion

3.1. Radio/X-ray Comparison

As shown in Figure 3, diffuse radio emission seen in the vicinity of the pulsar closely matches the extent of the diffuse X-ray PWN (feature C in Figure 2). It thus seems clear that this radio emission is the long-sought radio PWN. An elongated region of reduced radio emission can be seen to the south of the pulsar, corresponding closely to the morphology of the X-ray “jet” (feature D). This argues that this is a physically distinct structure within the nebula, and does not simply result from variations in brightness.

3.2. The Diffuse Nebula

The X-ray emission surrounding B1509–58 shows a clear symmetry axis, oriented at a position angle $150^\circ \pm 5^\circ$ (N through E), and manifested on all spatial scales between $10'' = 0.2$ pc and $10' = 15$ pc. Such alignment can only be enforced by the central pulsar. We think it likely that this axis represents the spin-axis of the pulsar, as has also been argued for the Crab and Vela pulsars (Hester et al. 1995; Helfand, Gotthelf & Halpern 2001).

A variety of different arguments imply that the magnetic field in the PWN is approximately $8 \mu\text{G}$ (see Gaensler et al. 2002 for details). This is an order of magnitude weaker than in the Crab Nebula, and implies a spectral break due to synchrotron cooling just below the X-ray band. This low magnetic field is most likely a result of the low density of the medium into which the PWN has expanded (Bhattacharya 1990). It is unlikely the pulsar is much older than τ (e.g. Gvaramadze, these proceedings), as this would require an even lower nebular field strength, not consistent with other estimates.

3.3. Outflow and Orientation

Feature D has a distinctly harder synchrotron spectrum than the surrounding PWN. If the injected electron spectrum in the two regions is the same and the spectral difference between them is due to synchrotron cooling, it can be shown that the flow velocity in feature D must be $> 0.2c$ (Gaensler et al. 2002). Thus this source corresponds to a true jet, which we have calculated carries away $> 0.5\%$ of \dot{E} . This jet is directed along the pulsar spin-axis, and appears to be a much larger and more spectacular version of similar features seen for the Crab and Vela PWNe (Hester et al. 1995; Helfand et al. 2001).

While no direct counterpart to this outflow can be seen to the north of the pulsar, the collimated nature of feature E suggests that we are seeing a cylindrical sheath of emission around an unseen counter-jet. This lack of direct emission can be simply explained by Doppler boosting, provided the jet axis is inclined by $\zeta \lesssim 30^\circ$ to the line-of-sight. This is contrary to the edge-on morphology, $\zeta \sim 70^\circ$, argued by Brazier & Becker (1997) from lower-resolution data.

3.4. Arcs and Inner Structure

Feature F is distinctly one-sided, and so can potentially be interpreted as a bow-shock driven by the pulsar. However, this feature is embedded within a much larger PWN, in which the pulsar’s velocity cannot be supersonic.

We thus prefer to interpret this arc as a toroidal structure, lying in a plane perpendicular to the main symmetry axis. In this case, the projected morphology of the arc implies $\zeta < 30^\circ$, consistent with the estimate made above from Doppler boosting of the jet.

Considered together, the inner and outer arcs (features I and F respectively) resemble the inner ring and outer torus seen in *Chandra* images of the Crab Nebula (Weisskopf et al. 2000; Mori, these proceedings). There are two characteristic time-scales associated with such structures: the time-scale for radiative losses via synchrotron emission, and the flow time from the pulsar. In the torus of the Crab Nebula, these times are comparable. However, for PSR B1509–58 the radiative time-scale is ~ 30 times longer than the flow time due to the lower

nebular magnetic field. Thus the arcs seen here must be dynamical, not radiative, features in the PWN. We show elsewhere that they can be interpreted as “wisps” as seen in the Crab Nebula, resulting from ion compression in a particle-dominated flow (Arons, these proceedings; Gaensler et al. 2002). In this case, we might expect outward motion of these features as is seen for the Crab. The expected proper motion would be a few arcsec per year, easily detectable with *Chandra*.

An interpretation for the knots close to the pulsar (features 2–5) is less clear. These knots may be emission from the unshocked pulsar wind, analogous to “knot 1” and “knot 2” seen with *HST* close to the Crab pulsar (Hester et al. 1995).

4. Conclusion and Questions

These *Chandra* data have provided a wealth of new information on PSR B1509–58 and its interaction with its environment. We have confirmed the presence of a collimated flow directed along the pulsar spin-axis, and have argued that the flow is relativistic and is inclined at $< 30^\circ$ to our line-of-sight. We have interpreted two arcs of emission seen close to the pulsar as dynamical features in an equatorial flow, and have identified several knots at separations < 0.5 pc from the pulsar.

Many issues still need to be investigated. Do the arcs and knots show motion and/or variability? Do any of these features have counterparts at other wavelengths? What is the nature of RCW 89 and its thermal clumps? While these questions still remain, it is clear that PSR B1509–58 provides a new opportunity to probe the detailed structure of a pulsar wind.

Acknowledgments. This work was supported by NASA through SAO grant GO0-1134X, Hubble Fellowship grant HST-HF-01107.01-A (B.M.G.), contracts NAS8-37716 and NAS8-38252 (M.J.P.), and LTSA grant NAG5-8063 (V.M.K.).

References

- Bhattacharya, D. 1990, *J. Astrophys. Astron.*, 11, 125
 Brazier, K. T. S., & Becker, W. 1997, *MNRAS*, 284, 335
 Dubner, G. M., et al. 2002, *AJ*, in press (astro-ph/0110218)
 Gaensler, B. M., et al. 1999, *MNRAS*, 305, 724
 Gaensler, B. M., et al. 2002, *ApJ*, submitted (astro-ph/0110454)
 Greiveldinger, C., et al. 1995., *ApJ*, 454, 855
 Helfand, D. J., Gotthelf, E. V., & Halpern, J. P. 2001, *ApJ*, 556, 380
 Hester, J. J., et al. 1995, *ApJ*, 448, 240
 Manchester, R. N., & Durdin, J. M. 1983, *IAU Symposium* 101, p421
 Tamura, K., Kawai, N., Yoshida, A., & Brinkmann, W. 1996, *PASJ*, 48, L33
 Trussoni, E., et al. 1996, *A&A*, 306, 581
 Weisskopf, M. C., et al. 2000, *ApJ*, 536, L81